Directional dependence of nonlinear surface acoustic waves in the (001) plane of cubic crystals

R. E. Kumon[a] and M. F. Hamilton
Department of Mechanical Engineering, The University of Texas at Austin, Austin, Texas 78712-1063

(Received 16 August 2001; revised 19 December 2001; accepted 7 January 2002)

Spectral evolution equations are used to perform analytical and numerical studies of nonlinear surface acoustic waves in the (001) plane of a variety of nonpiezoelectric cubic crystals. The basic theory underlying the model equations is outlined, and quasilinear solutions of the equations are presented. Expressions are also developed for a characteristic length scale for nonlinear distortion and a nonlinearity coefficient. A time-domain equation corresponding to the spectral equations is derived. Numerical calculations based on measured second- and third-order elastic constants taken from the literature are performed to predict the evolution of initially monofrequency surface waves. Nonlinearity matrix elements that indicate the coupling strength of harmonic interactions are shown to provide a useful tool for characterizing waveform distortion. The formation of compression or rarefaction shocks can be strongly dependent on the direction of propagation, and harmonic generation is suppressed or increased in certain directions. © *2002 Acoustical Society of America.*
[DOI: 10.1121/1.1455023]

PACS numbers: 43.25.Fe, 43.25.Dc [ANN]

I. INTRODUCTION

Unlike the theory for nonlinear Rayleigh waves in isotropic media, the theory for nonlinear surface acoustic waves (SAWs) in crystalline media predicts a wide diversity of effects that depend on the elastic and symmetry parameters of the materials, orientation of the surface cut with respect to the crystalline axes, and direction of propagation. Simulations based on numerical solution of spectral evolution equations introduced by Hamilton, Il'inskii, and Zabolotskaya[1] are presented for eight different crystals (KCl, NaCl, SrF_2, BaF_2, Si, Ge, Ni, Cu) over a full range of propagation directions in the (001) surface cut (results for additional cubic crystalline materials and symmetries are presented elsewhere[2]). The nonlinearity matrix used to describe harmonic interactions generally has complex-valued elements with nonuniform phase for an arbitrary surface cut. However, because of the symmetries in the (001) surface cut of cubic crystals, the nonlinearity matrix for this plane can always be written in a real-valued form, similar to that for the case of nonlinear Rayleigh waves. While the qualitative nature of the waveform distortion of surface waves in the (001) plane is similar to that of nonlinear Rayleigh waves in some cases, the simulations show that the distortion may depend strongly on the direction of propagation. For example, compression shocks may form in some directions but rarefaction shocks in others. In addition, there exist particular directions where the distortion differs completely from nonlinear Rayleigh waves because of suppression or enhancement of generation of one or more harmonics. Measurements in crystalline silicon corroborate several of the predicted results.[3]

While extensive work has been performed to investigate nonlinear surface waves,[4,5] most of it has been limited to isotropic media. Researchers first began to develop theories to predict the propagation of nonlinear SAWs in nonpiezoelectric crystals in the mid-1980s. Planat[6] developed a theory for an elastic solid with general anisotropy based on a multiple scales approach but presented results for only a limited number of harmonics. Another multiple scales theory with general anisotropy by Lardner[7] was employed by Lardner and Tupholme[8] to investigate the properties of nonlinear surface waves in cubic crystals, but the reported results were limited to propagation along a crystalline axis in a plane of symmetry. Results were provided as tables of coefficients describing the growth and decay rates of the fundamental, second, and third harmonics for 35 cubic crystals or crystalline alloys, as well as for the first three harmonic propagation curves for the specific case of magnesium oxide. Independently, Parker[9] developed a theory for nonpiezoelectric, anisotropic media that avoids some of the complications and limitations of the multiple scales approach by introducing a reference frame moving at the linear wave speed to derive spectral evolution equations. Results were given only in terms of waveforms for an isotropic solid (although numerical results were later presented for a piezoelectric crystal[10]).

During the mid-1990s, Hamilton *et al.*[1,11] extended the isotropic theory of Zabolotskaya for nonlinear Rayleigh waves[12,13] to include nonpiezoelectric, anisotropic media and presented results for potassium chloride in selected propagation directions. Piezoelectric effects were subsequently included in this theory.[14] Gusev *et al.*[15] also developed a theory for nonlinear SAWs in anisotropic media, but numerical calculations demonstrating their results have not been reported. Their evolution equations are given in the time domain and differ from those of Parker[9] and Hamilton *et al.*[1] Further discussion of the approach used by Gusev *et al.*[15] is provided by Meegan *et al.*[16]

In recent experiments, very-high-amplitude SAWs

[a]Current address: National Institute of Standards and Technology, 325 Broadway, Mail Stop 853, Boulder, CO 80305-3328. Electronic mail: kumon@mailaps.org

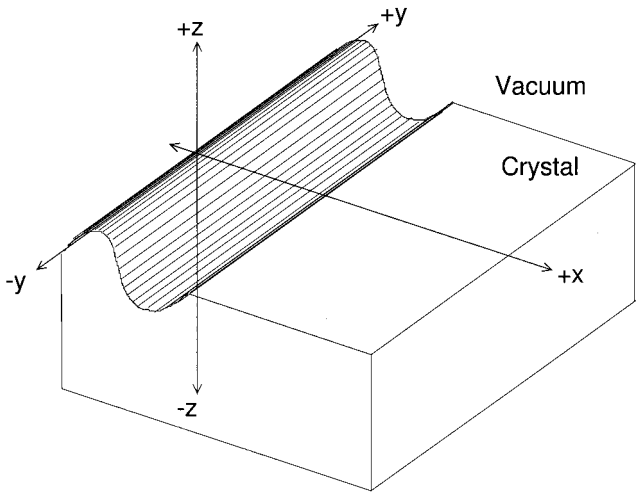

FIG. 1. Coordinate system for plane surface wave propagation. Note that the positive z axis points out of the crystal.

(strains up to 0.01) have been generated photoelastically in fused quartz,[17–19] polycrystalline aluminum and copper,[20] and crystalline silicon[17,21] via pulsed laser excitation. Calculations based on the theories of Zabolotskaya[12] for isotropic media and Hamilton *et al.*[1] for crystals agree well with the measured results.[3,22,23]

II. NONLINEAR THEORY

A. Model equations

A plane surface wave is assumed to propagate in the x direction in an anisotropic half-space $z \leqslant 0$ (see Fig. 1). The velocity components of the surface wave are taken to have the form

$$v_j(x,z,\tau) = \sum_{n=1}^{\infty} v_n(x) u_{nj}(z) e^{-in\omega\tau} + \text{c.c.}, \tag{1}$$

where $j = x,y,z$ is the coordinate index, ω is the fundamental angular frequency in the expansion, $\tau = t - x/c$ is the retarded time, and c is the linear wave speed in the direction of propagation. The depth dependence is given by the functions

$$u_{nj}(z) = \sum_{s=1}^{3} \beta_j^{(s)} e^{ink\zeta_s z}, \tag{2}$$

where ζ_s and $\beta_j^{(s)}$ are computed from the eigenvalues and eigenvectors, respectively, of the linear boundary value problem corresponding to the stress-free surface,[24] and $k = \omega/c$ is the fundamental wave number. The coupled spectral evolution equations for the slowly varying amplitudes $v_n(x)$ are given by[1]

$$\frac{dv_n}{dx} + \alpha_n v_n = \frac{n^2\omega}{2\rho c^4}\left(\sum_{m=1}^{n-1} S_{m,n-m} v_m v_{n-m} - 2 \sum_{m=n+1}^{\infty} S^*_{n,m-n} v_m v^*_{m-n} \right), \tag{3}$$

where α_n is the absorption coefficient for the nth harmonic, ρ is the density, and S_{lm} is the nonlinearity matrix. Equations (3) are written in terms of Lagrangian coordinates, an approach which is convenient for describing the surface boundary conditions. The nonlinearity matrix is given by

$$S_{lm} = \sum_{s_1,s_2,s_3=1}^{3} \frac{F_{s_1 s_2 s_3}}{l\zeta_{s_1} + m\zeta_{s_2} - (l+m)\zeta^*_{s_3}}, \tag{4}$$

where

$$F_{s_1 s_2 s_3} = \tfrac{1}{2} d'_{ijklmn} \beta_i^{(s_1)} \beta_k^{(s_2)} [\beta_m^{(s_3)}]^* l_j^{(s_1)} l_l^{(s_2)} [l_n^{(s_3)}]^*, \tag{5}$$

$$d'_{ijklmn} = d_{ijklmn} + c_{ijln}\delta_{km} + c_{jnkl}\delta_{im} + c_{jlmn}\delta_{ik}, \tag{6}$$

$\mathbf{l}^{(s)} = (1,0,\zeta_s)$, and c_{ijkl} and d_{ijklmn} are the second-and third-order elastic constants transformed to the chosen reference frame. (Elastic constants are typically listed with respect to the coordinate system defined by the crystalline axes.)

The following source conditions are assumed at $x = 0$:

$$v_1 = v_0, \quad v_{n>1} = 0, \tag{7}$$

where v_0 is taken to be a real-valued characteristic amplitude. Substitution of Eqs. (7) into (1) and (2) yields the following source velocity components at the surface:

$$v_j(0,0,t) = 2v_0 |B_j| \cos(\omega t - \phi_j), \tag{8}$$

where

$$B_j = |B_j| e^{i\phi_j} = \sum_{s=1}^{3} \beta_j^{(s)}. \tag{9}$$

Note that only the relative phases of B_j are determined by the theory[1]—the absolute phases may be chosen as is convenient. While all simulations considered in this paper are for a sinusoidal source, any source spectrum can be employed via Fourier decomposition. For the simulations shown here, the absolute phases are chosen such that B_1 lies along the negative imaginary axis. In the limit of an isotropic solid we may choose $v_y = 0$, and Eqs. (8) reduce to

$$\begin{aligned} v_x(0,0,t) &= -2v_0 |B_1| \sin\omega t, \\ v_z(0,0,t) &= 2v_0 |B_3| \cos\omega t. \end{aligned} \tag{10}$$

B. Second harmonic and nonlinearity coefficient

To gain insight into the nature of the lowest-order harmonic generation, consider Eqs. (3) with ∞ in the second summation replaced by 2:

$$\frac{dv_1}{dx} + \alpha_1 v_1 = 0, \quad \frac{dv_2}{dx} + \alpha_2 v_2 = \frac{2S_{11}\omega}{\rho c^4} v_1^2, \tag{11}$$

and the corresponding solutions satisfying Eqs. (7):

$$v_1 = v_0 e^{-\alpha_1 x}, \quad v_2 = \frac{2S_{11}\omega v_0^2}{\rho c^4}\left(\frac{e^{-2\alpha_1 x} - e^{-\alpha_2 x}}{\alpha_2 - 2\alpha_1} \right). \tag{12}$$

Note that S_{11} is generally complex-valued, and thus $S_{11}/|S_{11}| = e^{i\psi_{11}}$ with $0 \leqslant \psi_{11} \leqslant 2\pi$. In the limit of no absorption Eqs. (12) reduce to

$$v_1/v_0 = 1, \quad v_2/v_0 = (2S_{11}\omega v_0^2/\rho c^4)x. \tag{13}$$

The similarity of Eqs. (13) with the corresponding solutions for sound waves in lossless fluids makes it possible to propose an estimate of the shock formation distance. Let $\overline{x_f}$

be the shock formation distance for a finite-amplitude sound wave radiated at angular frequency ω and velocity amplitude v_0 in a lossless fluid. The quasilinear solution for the second harmonic component is[25] $|v_2|/v_0 = x/2\overline{x_f}$. Comparison with Eqs. (13) shows that an estimate of the shock formation distance x_0 for the SAW is thus

$$x_0 = \frac{\rho c^4}{4|S_{11}|\omega v_0}, \tag{14}$$

which depends on the third-order elastic constants via the nonlinearity matrix element S_{11}.

Equation (14) can be somewhat problematic when applied to crystalline media. Harmonic generation may occur while shock formation does not, and therefore the characteristic distance given by Eq. (14) loses meaning in those cases. For example,[1] near the ⟨100⟩ direction in the (001) cut of KCl, the transfer of energy from the fundamental to higher harmonics is so weak that shocks never form (see Sec. III B 3). Despite the fact that Eq. (14) is not applicable in all cases, it does provide at least a first-order estimate of the shock formation distance in many cases of interest and can still be useful in this respect.

An expression for a nonlinearity coefficient similar to that of fluids may also be derived. For a finite-amplitude wave radiated at angular frequency ω and velocity amplitude v_0 propagating in such a medium, the shock formation distance $\overline{x_f}$ is related[25] to the coefficient of nonlinearity β_f by $\overline{x_f} = c^2/|\beta_f|v_0\omega$. From Eq. (14), a comparable SAW nonlinearity coefficient is

$$\beta = -4S_{11}/\rho c^2. \tag{15}$$

In general, β is complex-valued, although cases do exist where it is strictly real-valued. The negative sign is introduced in Eq. (15) so that the sign of the nonlinearity coefficient is consistent with the corresponding theory for isotropic media.[26]

C. Time-domain evolution equation

As for isotropic solids,[12] a time-domain equation for the evolution of nonlinear SAWs on the surface of crystals ($z=0$) may be derived from the frequency-domain evolution equations, Eqs. (3), without the absorption term. Equations (3) may be rewritten with the summation on the right side performed over all indices, both positive and negative:

$$\frac{dv_n}{dx} = \frac{n^2\omega}{2\rho c^4} \sum_{l+m=n} \frac{lm}{|lm|} S_{lm} v_l v_m. \tag{16}$$

From Eqs. (1) at $z=0$ we have

$$v_j(x,\tau) = \sum_n v_{nj}(x) e^{-in\omega\tau}, \tag{17}$$

where $v_{nj} = v_n(x)|B_j|e^{i\phi_j \operatorname{sgn} n}$. The spectral component with $n=0$ is zero because the bulk of the solid is assumed to be at rest. Following the approach for isotropic media,[27] it can be shown that

$$\frac{\partial v_j}{\partial x} = \frac{C}{c^2T^2} \frac{\partial}{\partial \tau} \int \int_{-T/2}^{T/2} L(\phi_j, \tau-\tau', \tau-\tau'') \times v_j(x,\tau') v_j(x,\tau'')\, d\tau'\, d\tau'', \tag{18}$$

where $T = 2\pi/\omega$ and $C = -1/2\rho c^2|B_j|$. The kernel of the integral is

$$L(\phi_j, \tau', \tau'') = \sum_{l,m} P_{lm}(\phi_j) Q_{lm}(\phi_j) S_{lm} e^{-il\omega\tau'} e^{-im\omega\tau''}, \tag{19}$$

where

$$P_{lm}(\phi_j) = i(l+m) e^{i\phi_j \operatorname{sgn}(l+m)}, \tag{20a}$$

$$Q_{lm}(\phi_j) = -\operatorname{sgn}(lm) e^{-i\phi_j \operatorname{sgn} l} e^{-i\phi_j \operatorname{sgn} m}. \tag{20b}$$

As mentioned in Sec. II A, linear theory determines only the relative phases of the B_j. Without loss of generality, choose the absolute phase of one velocity component v_{j_0} (i.e., set j equal to a specific index we shall call j_0) to be a negative imaginary number so that the result corresponds to the phase convention used previously in the theory for isotropic media.[12] Under this condition, the kernel can be shown[2] to reduce to

$$L(\phi_{j_0} = -\pi/2, \tau', \tau'') = \sum_{l,m} |l+m| S_{lm} e^{-i\omega\tau'} e^{-im\omega\tau''}. \tag{21}$$

Other velocity components (for which $j \neq k$) may be obtained from integral transforms of the $v_j(x,\tau)$ component. From Eqs. (17), it follows that the nth spectral amplitudes of the jth and kth velocity components are related by

$$v_{nk}(x) = \begin{cases} (B_k/B_j) v_{nj}(x) & \text{for } n>0, \\ (B_k^*/B_j^*) v_{nj}(x) & \text{for } n<0, \end{cases} \quad (j \neq k). \tag{22}$$

Equations (22) imply that the velocity waveform components in the x_j and x_k directions are related by[15]

$$v_k(x,\tau) = \operatorname{Re}(B_k/B_j) v_j(x,\tau) - \operatorname{Im}(B_k/B_j) \mathcal{H}[v_j(x,\tau)], \tag{23}$$

where

$$\mathcal{H}[f(\tau)] = \frac{1}{\pi} Pr \int_{-\infty}^{\infty} \frac{f(\tau')}{\tau'-\tau} d\tau' \tag{24}$$

defines the Hilbert transform, and Pr indicates the Cauchy principal value of the integral.

III. NUMERICAL RESULTS

The focus of this article is the propagation of nonlinear surface waves in cubic crystals. Cubic crystals are chosen not because of any limitation of the underlying theory [Eqs. (1)–(6) apply for arbitrary anisotropy], but because they exhibit the simplest types of fully three-dimensional anisotropy, and there is considerable experimental data available for their material properties, especially higher-order elastic constants. Eight nonpiezoelectric crystals were chosen for study to provide a variety of anisotropy ratios.

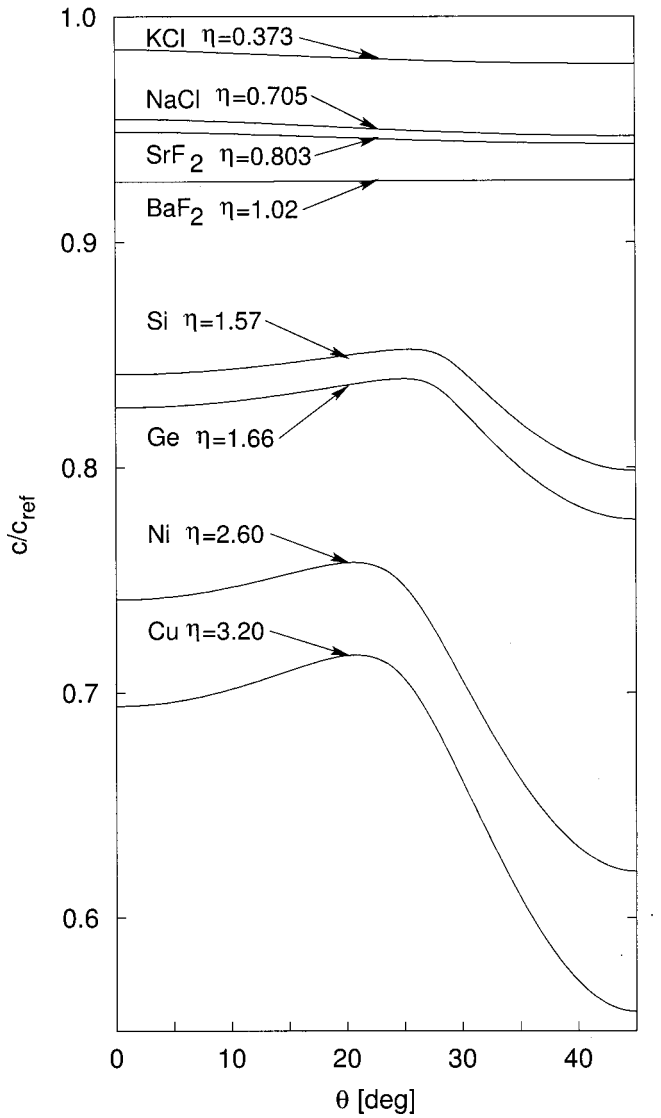

FIG. 2. Dependence of SAW speed on direction of propagation in the (001) plane for selected materials. The SAW speed of each material is measured relative to $c_{\text{ref}}=(c_{44}/\rho)^{1/2}$, and the angle θ gives the direction of the wave vector relative to $\langle 001\rangle$. Because of the symmetries of this cut, the wave speeds are symmetric about $\theta=45°$ and periodic every $\Delta\theta=90°$.

A. Linear effects

The variation of the linear wave speed as a function of angle may be characterized by the anisotropy ratio[24]

$$\eta=\frac{2c_{66}}{c_{11}-c_{12}}, \tag{25}$$

where $c_{66}=c_{44}$ for cubic symmetry. This definition is constructed such that $\eta=1$ for an isotropic material. The SAW speeds for many materials group conveniently by anisotropy ratio. A larger anisotropy ratio implies a slower SAW speed relative to the fast transverse bulk wave speed. Because of this grouping, selected materials can be shown to be characteristic of many others.[24]

Figure 2 shows the SAW speed of selected materials as a function of propagation direction. These curves were computed using density data from review articles by Pies *et al.*[28] and Eckerlin *et al.*,[29] and second-order elastic constant data from a review article by Hearmon.[30] The direction of propagation is measured by angle θ from $\langle 100\rangle$, and the wave speed for each material is scaled by $c_{\text{ref}}=(c_{44}/\rho)^{1/2}$ for that material. For the (001) surface cut, c_{ref} is also the speed of the fast transverse bulk wave, which is constant for all directions in this plane. Because the normal to the (001) plane is a fourfold symmetry axis, the SAW speed is periodic every $\Delta\theta=90°$. In addition, the $\langle 110\rangle$ direction is a twofold symmetry axis, and therefore the SAW speed is symmetric about that direction ($\theta=45°$ in Fig. 2). In most cases (and for all cases shown here) the speeds group by anisotropy ratio, with materials possessing lower anisotropy ratios having higher relative SAW speeds. Materials with $\eta\approx 1$ are nearly isotropic and hence have nearly constant SAW speed for all directions.

For all materials, the direction $\theta=0°$ is a pure mode, and the particle trajectories are confined to the sagittal plane. Some materials have additional pure modes in other directions, but in these cases the SAW often has a transverse component (e.g., Ni, Cu, Si, Ge). In some materials, the SAW speed approaches the transverse bulk wave speed as the direction approaches $\theta=45°$.[24] This effect is the source of the dip in the SAW speeds of Ni, Cu, Si, and Ge observed in Fig. 2. The SAW becomes a shear horizontal bulk wave at $\theta=45°$, and the degeneracy gives rise to a pseudosurface wave mode in the same direction. Because the nonlinear theory described above does not apply to pseudosurface waves, modes propagating in these directions are not considered further.

All of the aforementioned effects pertain to linear SAWs; they are mentioned here primarily to provide a context for the nonlinear effects discussed next.

B. Nonlinear effects

It is convenient to introduce the dimensionless quantities

$$V_n=v_n/v_0, \quad X=x/x_0, \quad A_n=\alpha_n x_0, \tag{26}$$

where v_0 is a characteristic velocity of the SAW and x_0 is given by Eq. (14). Equation (3) becomes

$$\frac{dV_n}{dX}+A_nV_n=\frac{n^2}{8|S_{11}|}\left(\sum_{m=1}^{n-1}S_{m,n-m}V_mV_{n-m}-2\sum_{m=n+1}^{N}S^*_{n,m-n}V_mV^*_{m-n}\right), \tag{27}$$

where N is the number of harmonics retained in the calculation. The boundary conditions corresponding to Eq. (7) are

$$V_1=1, \quad V_{n>1}=0. \tag{28}$$

It also proves useful to define the dimensionless nonlinearity matrix

$$\hat{S}_{lm}=-S_{lm}/c_{44}. \tag{29}$$

The negative sign is introduced to be consistent in sign with the nonlinearity matrix elements R_{lm} used for nonlinear Rayleigh waves.[31] In all cases, the figures throughout this article report matrix elements defined by Eq. (29). Because the

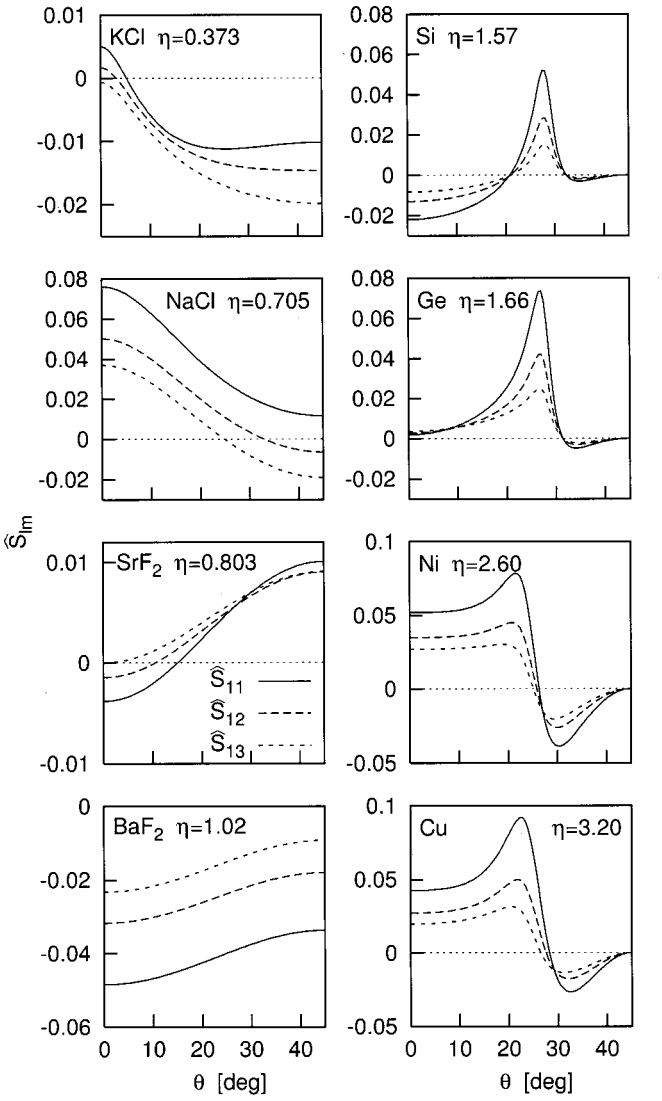

FIG. 3. Dependence of nonlinearity matrix elements on direction of propagation in the (001) plane in selected materials. The solid, long-dashed, and short-dashed lines correspond to $\hat{S}_{11}$, $\hat{S}_{12}$, and $\hat{S}_{13}$, respectively.

(001) surface is a plane of mirror symmetry, the nonlinearity matrix coefficients are all real-valued.

1. General study

Figure 3 shows plots of the nonlinearity matrix elements for a variety of crystals. Each graph plots $\hat{S}_{11}$ (solid), $\hat{S}_{12}$ (long-dashed), and $\hat{S}_{13}$ (short-dashed) over the range of directions $\theta=0°$ to $\theta=45°$. While plotting only three elements of the nonlinearity matrix certainly does not provide a full description of the nonlinear properties of the SAW, it can give a good idea of the evolution in many cases, as shown later. Moreover, the leading order terms in perturbation solutions for second, third, and fourth harmonic generation are proportional to $\hat{S}_{11}$, $\hat{S}_{12}$, and $\hat{S}_{13}$, respectively.

Four groups of crystals are shown in Fig. 3, with two different materials of similar structure in each group. The materials are ordered by increasing anisotropy ratio from top to bottom within each column (recall Fig. 2). The densities and second-order elastic constants used to construct Fig. 3 are the same as in Fig. 2, and the third-order elastic constants are listed in Table I.[32–36]

The first column of Fig. 3 shows the nonlinearity matrix elements for materials with η less than or approximately equal to unity: KCl, NaCl, SrF_2, BaF_2 ($\eta=0.373$, 0.705, 0.803, 1.02, respectively). The second column shows the nonlinearity matrix elements for materials with η greater than unity: Si, Ge, Ni, Cu ($\eta=1.57$, 1.66, 2.60, 3.20, respectively). Note that at $\theta=45°$, where the SAW and shear modes converge, $|\hat{S}_{lm}|\to 0$ in these materials. Si and KCl are chosen for investigation in detail in Secs. III B 2 and III B 3, respectively, because they provide examples of the different kinds of waveform distortion exhibited by nonlinear SAWs in the (001) plane.

2. Detailed study of silicon

Figure 4 (expanded from Fig. 3) shows the plot of $\hat{S}_{lm}$ for Si divided into three regions. The small circles on the curves correspond to the angles $\theta=0°$, 26°, and 35° discussed in detail below. In region I ($0°\leqslant\theta\leqslant 20.8°$) the nonlinearity is negative ($\hat{S}_{lm}<0$). As is shown below, this means that positive segments of the longitudinal particle velocity waveform steepen backward in space, and negative segments steepen forward (i.e., opposite to what a sound wave does in a fluid). In region II ($20.8°<\theta<32.3°$) the nonlinearity is positive ($\hat{S}_{lm}>0$), with waveform distortion the reverse of the first region. In region III ($32.3°<\theta\leqslant 45°$) the nonlinearity is again negative, although relatively weak. Observe that the linear wave speed varies by approximately 2% (see Fig. 2) over the angular range shown, whereas the changes in the nonlinearity matrix elements are of order unity. Hence not only do the nonlinear matrix elements change sign (with distinctly different waveform evolution as a result), but they also vary more widely in magnitude.

TABLE I. Third-order elastic (TOE) constants for selected nonpiezoelectric crystals. The constants are given relative to the reference frame defined by the crystalline axes in Voigt's notation with units of GPa.

Material	d_{111}	d_{112}	d_{123}	d_{144}	d_{155}	d_{156}	Source
KCl	−726	−24	+11	+23	−26	+16	Drabble *et al.* (Ref. 32)
NaCl	−843	−50	+46	+29	−60	+26	Drabble *et al.* (Ref. 32)
SrF_2	−821	−309	−181	−95.1	−175	−42.1	Alterovitz *et al.* (Ref. 33)
BaF_2	−584	−299	−206	−121	−88.9	−27.1	Gerlich (Ref. 34)
Si	−825	−451	−64	+12	−310	−64	McSkimin *et al.* (Ref. 35)
Ge	−710	−389	−18	−23	−292	−53	McSkimin *et al.* (Ref. 35)
Ni	−2032	−1043	−220	−138	−910	+70	Salama *et al.* (Ref. 36)
Cu	−1390	−778	−181	−140	−648	−16	Salama *et al.* (Ref. 36)

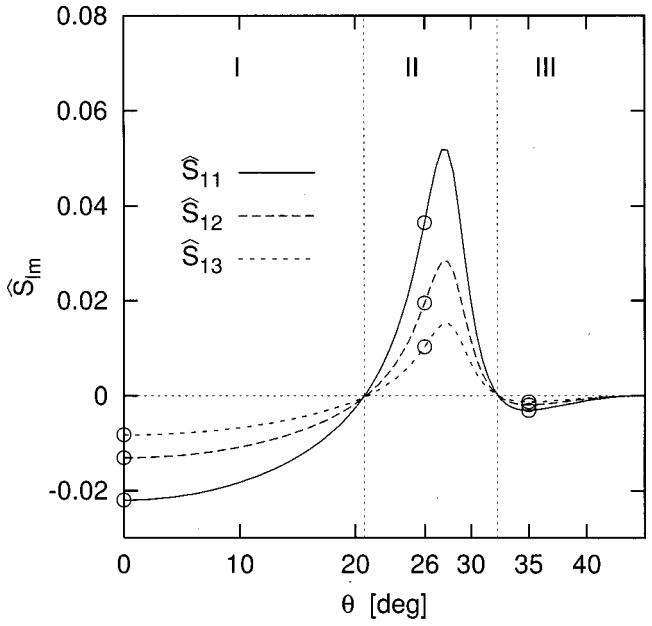

FIG. 4. Nonlinearity matrix elements $\hat{S}_{11}$, $\hat{S}_{12}$, $\hat{S}_{13}$ for Si in the (001) plane as a function of direction. Because of the symmetries of this cut, the matrix elements are symmetric about $\theta=45°$ and periodic every $\Delta\theta=90°$. The circled directions are discussed in detail in the text.

Observe that the weakening in the third region is coincident with the gradual convergence of the SAW mode and transverse bulk mode into a shear horizontal bulk wave, as seen from the wave speed plot in Fig. 2. Additional calculations[2] indicate that an increasing amount of energy moves away from the surface and into the bulk of the solid as the $\theta=45°$ direction is approached. As a result, it becomes increasingly difficult to create the surface amplitudes necessary to observe nonlinear effects in this SAW mode. (There does, however, exist a pseudosurface wave mode at a higher wave speed,[24] and it is this mode which is often excited experimentally in this region.)

Finally, Fig. 4 indicates that $\hat{S}_{11}$, $\hat{S}_{12}$, and $\hat{S}_{13}$ pass through zero near $\theta\simeq20.8°$ and $\theta\simeq32.3°$. Additional calculations show that while all matrix elements do not go through zero at the same angle, all significant elements are close to zero at these angles. Hence propagation is expected to be nearly linear in both these directions even for finite-amplitude waves. Because harmonic generation is suppressed, shocks do not form, or they form only over very large distances.

To investigate the effects of the sign and magnitude of $\hat{S}_{lm}$ on the velocity waveforms, simulations were performed by solving the system given by Eqs. (27) for the monofrequency source condition given in Eq. (28). The equations were integrated numerically using a fourth-order Runge-Kutta routine with $N=200$ harmonics (i.e., $1<n<N$, with $V_{-n}=V_n^*$). The nondimensional distance $X=x/x_0=1$ corresponds to approximately one shock formation distance. The absorption coefficients were chosen by assuming classical absorption due to viscosity and heat conduction, for which the quadratic frequency dependence $A_n=n^2A_1$ is obtained. The absorption for the fundamental was selected to be $A_1=\alpha_1x_0=0.025$ to make the absorption length much larger than the shock formation distance. The effect of the absorption is then weak in comparison to that of the nonlinearity, and its primary influence is on the rise time of the shock. Once the spectra were generated, the waveforms were reconstructed using Eq. (1).

Figure 5 displays the simulation results for one direction in each region of Fig. 3. Each row shows waveform evolution in the direction specified by the angle listed in that row. The columns from left to right give the longitudinal, transverse, and vertical components of the velocity, respectively. In each direction, the waveforms are normalized such that $|V_x|^2+|V_y|^2+|V_z|^2=1$ at $X=0$, and hence the magnitudes for different directions should not be compared. Each graph of the velocity components contains waveforms at $X=0$ (short-dashed), $X=1$ (long-dashed), and $X=2$ (solid) in the retarded time frame, i.e., a frame moving at the linear SAW speed.

$\theta=0°$: This direction is in region I of Fig. 4, where the nonlinearity elements $\hat{S}_{11}$, $\hat{S}_{12}$, and $\hat{S}_{13}$ are negative. As mentioned previously, the longitudinal velocity waveform exhibits distortion with the peak receding and the trough advancing, opposite to that of a sound wave in a fluid. In addition, the longitudinal waveform exhibits the cusping near the shock front that is characteristic of SAWs. The vertical velocity waveform also exhibits the cusped peak seen in Rayleigh waves. In fact, SAWs in this direction are considered to be ''Rayleigh-type'' waves, as defined by Farnell,[24] for the following three reasons. First, due to the symmetries in this direction, $B_2=0$, and the motion is thus confined to the sagittal plane. Second, this is a pure mode direction. (Experimentally, pure mode directions are often preferred over other directions because it is typically easier to make measurements when the power flow is in the same direction as the wave vector.) Third, the principal axis of the surface particle trajectory is perpendicular to the free surface due to the 90° phase difference between B_1 and B_3. Thus, except for the fact that the amplitudes of the particle velocities do not decay purely exponentially into the solid, propagation in this direction is quite similar to the propagation of nonlinear Rayleigh waves in isotropic materials with negative nonlinearity coefficients (e.g., fused quartz[22]).

$\theta=26°$: This direction is in region II of Fig. 4, and it is the only direction in this region where there is a pure mode. $\hat{S}_{11}$, $\hat{S}_{12}$, and $\hat{S}_{13}$ are positive, and the longitudinal velocity waveform exhibits distortion with the peak of the wave advancing and the trough receding, opposite that in region I. Accordingly, the vertical velocity forms a cusped peak in the positive direction. Note that the horizontal scale has been shifted over by π rad in these waveforms, as compared to the $\theta=0°$ case.

$\theta=35°$: Here, and throughout region III of Fig. 4, $\hat{S}_{11}$, $\hat{S}_{12}$, and $\hat{S}_{13}$ are again negative, and the waveform distorts as in the $\theta=0°$ case. (Note that the horizontal scale has been shifted over by $-\pi$ rad, as compared to the $\theta=26°$ case, so as to be the same as in the $\theta=0°$ case.) This direction is not a pure mode, but it is the direction where the nonlinearity has the largest magnitude in this region. Even so, the magnitude

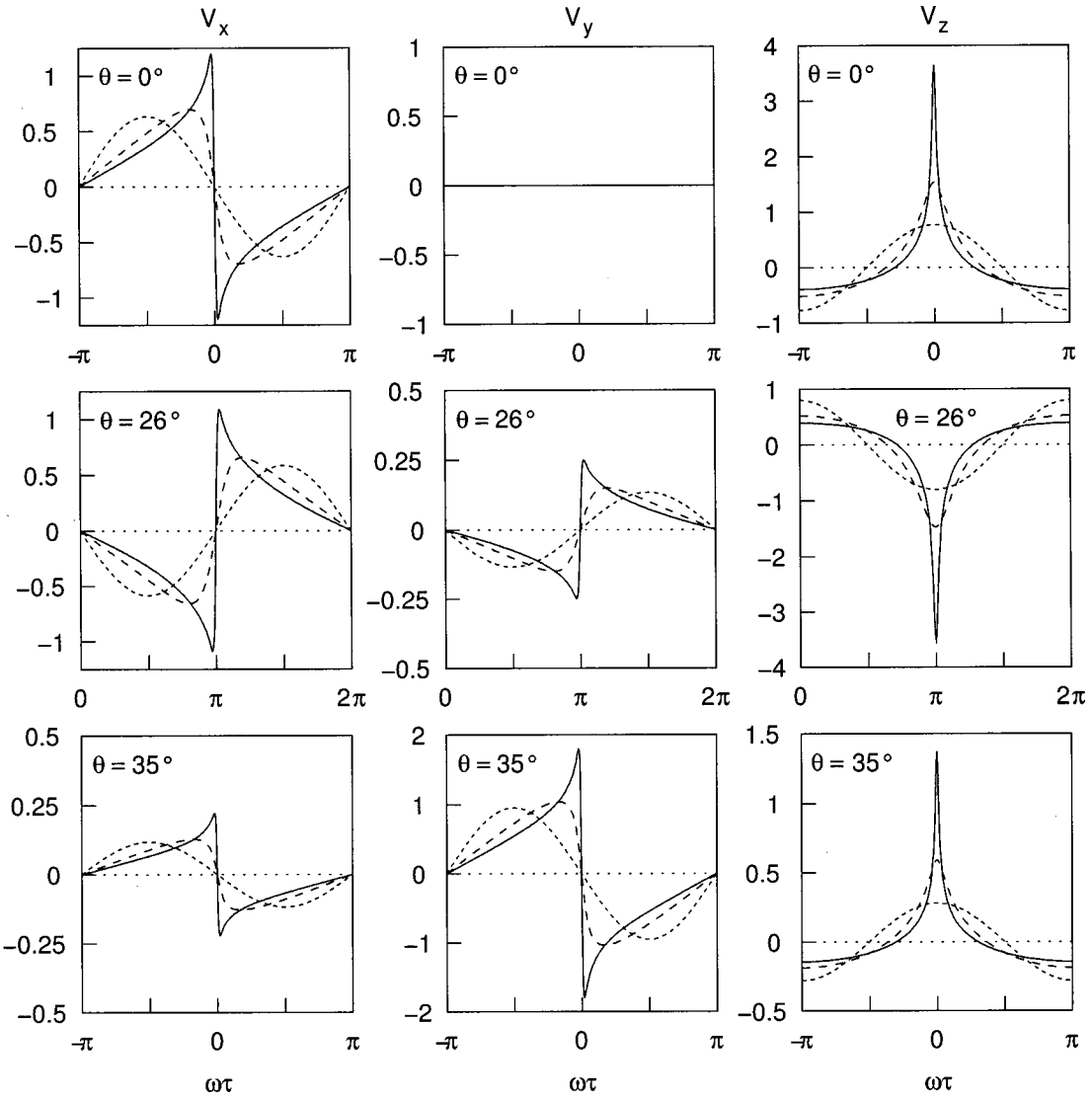

FIG. 5. Velocity waveforms in selected directions of propagation in the (001) plane of Si. The velocity components are normalized such that the initial amplitude satisfies $|V_x|^2+|V_y|^2+|V_z|^2=1$ in each propagation direction. The short-dashed, long-dashed, and solid lines correspond to propagation at distances $X=0$, $X=1$, and $X=2$, respectively.

of the nonlinearity is significantly weaker here than at $\theta=0°$, with $S_{11}(35°)/S_{11}(0°)\simeq 0.14$.

The simulations for Si presented above demonstrate both that the SAW nonlinearity varies significantly in magnitude and direction throughout the (001) cut, and that the nonlinearity matrix elements provide a map which can characterize the nature of the waveform distortion. Additional types of waveform distortion not exhibited in Si are shown in Sec. III B 3.

3. Detailed study of potassium chloride

The nonlinearity matrix elements $\hat{S}_{11}$, $\hat{S}_{12}$, and $\hat{S}_{13}$ for KCl are shown in Fig. 6 over the range $0°<\theta<10°$ (expanded in part from Fig. 3). The small circles on the curves correspond to the angles $\theta=0°$, 3.2°, and 10°, which are discussed in detail later in this work. As compared to the nonlinearity matrix elements for Si, the matrix elements for KCl are quantitatively and qualitatively different. At $\theta=0°$, $\hat{S}_{11}$ and $\hat{S}_{12}$ are positive while $\hat{S}_{13}$ is negative. As the angle from $\langle 100\rangle$ increases, $\hat{S}_{12}$ passes through zero around $\theta=3.2°$, and then finally $\hat{S}_{11}$ passes through zero around $\theta=5.2°$. The propagation at $\theta=5.2°$ is similar to that for $\theta=20.8°$ and $\theta=32.3°$ in Si, i.e., little harmonic generation occurs. At larger angles, the matrix elements $\hat{S}_{11}$, $\hat{S}_{12}$, and $\hat{S}_{13}$ are negative although, unlike Si, here the magnitude of $\hat{S}_{11}$ is less than the magnitudes of $\hat{S}_{12}$ and $\hat{S}_{13}$. Also unlike Si, the SAW modes do not converge with the transverse bulk mode at $\theta=45°$. Finally, here the percentage variation in the nonlinearity matrix elements as a function of angle again exceeds the corresponding variations in wave speed (compare with Fig. 2).

Figure 7 shows three additional types of velocity waveform distortion. Figure 7 has the same format as Fig. 5 except that the third and fourth columns show, respectively, the spectra at the locations corresponding to the waveforms, and the harmonic propagation curves for the first five harmonics. Also, the V_y waveforms are omitted because they are either zero or similar to the V_x waveforms.

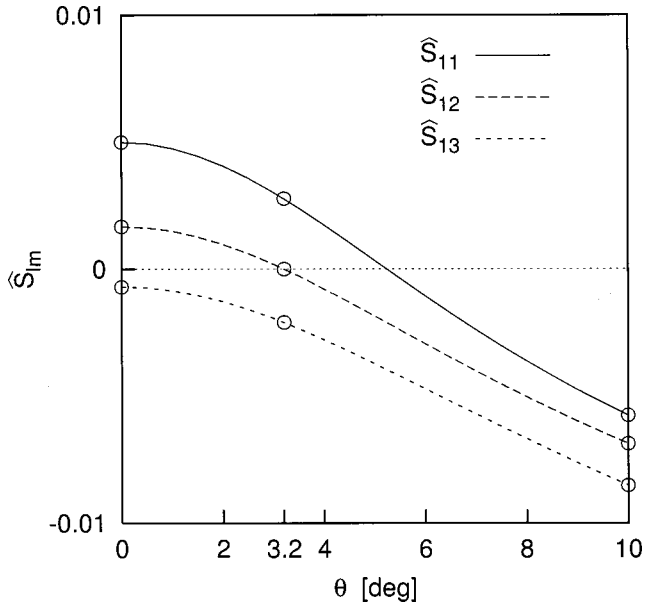

FIG. 6. Nonlinearity matrix elements $\hat{S}_{11}$, $\hat{S}_{12}$, $\hat{S}_{13}$ for KCl in the (001) plane as a function of direction. Because of the symmetries of this cut, the matrix elements are symmetric about $\theta=45°$ and periodic every 90°. The circled directions are discussed in detail in the text.

$\theta=0°$: In this direction, $\hat{S}_{11}$ and $\hat{S}_{12}$ are positive, and $\hat{S}_{13}\simeq-7.0\times10^{-4}$ is negative but close to zero and smaller than $\hat{S}_{11}$ and $\hat{S}_{12}$ in magnitude ($|\hat{S}_{13}|/|\hat{S}_{11}|\simeq0.14$, $|\hat{S}_{13}|/|\hat{S}_{12}|\simeq0.42$). The matrix element $\hat{S}_{13}$ indicates the coupling strength between the fundamental and third harmonic to generate the fourth harmonic. Energy that is transferred to the third harmonic from lower harmonics is therefore not as easily transferred to the fourth harmonic. The third harmonic (short-dashed) curve exceeds the second harmonic (long-dashed) in amplitude around $X=3$, while the fourth harmonic grows more slowly initially. Another consequence of a small value of $\hat{S}_{13}$ is that shock formation does not occur. For example, while the longitudinal waveform is distorting in a "positive" way, with peaks advancing and troughs receding, it has not yet formed a shock. Moreover, as seen in the frequency spectrum, relatively little energy is transferred to the higher spectral components as the wave propagates (contrast with the spectrum in the $\theta=10°$ direction). Additional calculations indicate that at distances $X>2$ the longitudinal velocity waveform steepens more but never forms a shock. Hence this is another direction at which shock suppression occurs. In contrast with Si, however, the harmonic suppression is less severe and occurs for a harmonic higher than the second.

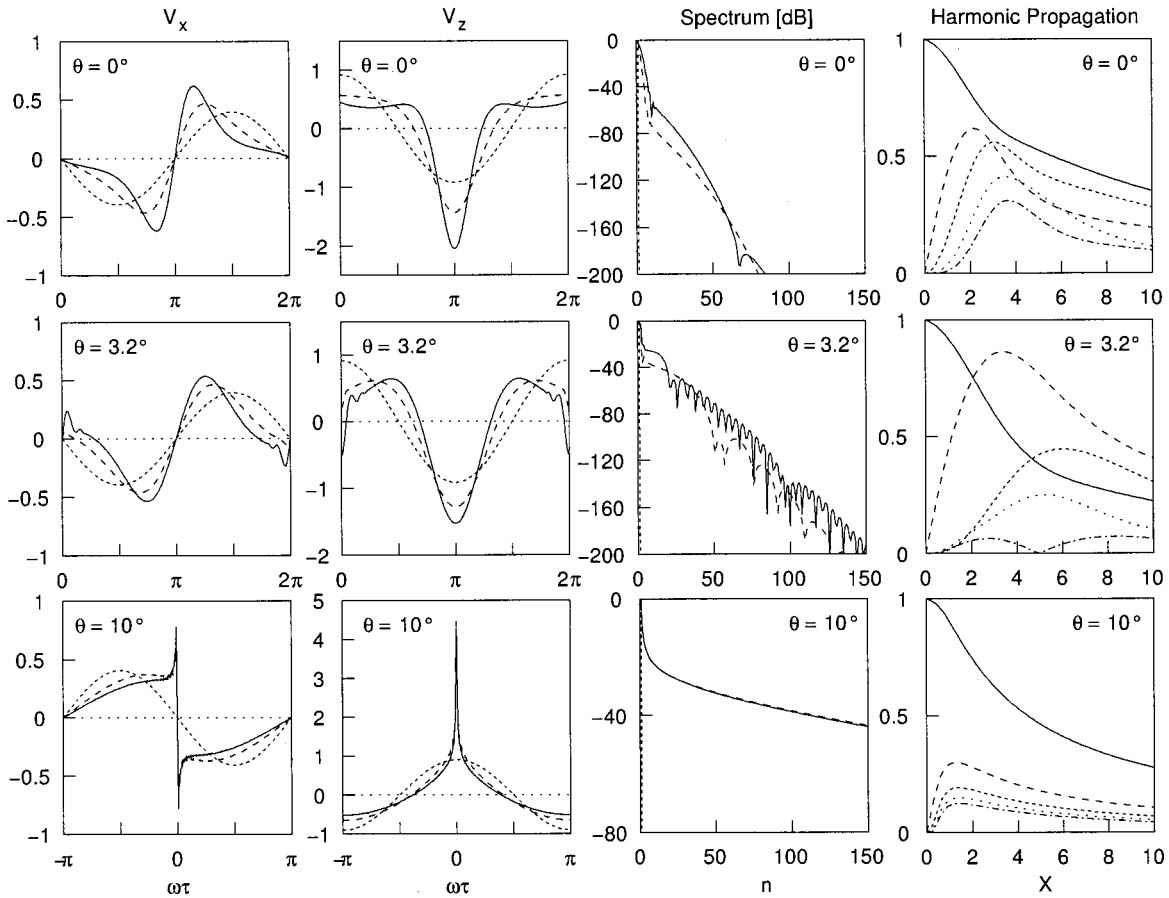

FIG. 7. Velocity waveforms in selected directions of propagation in the (001) plane of KCl. The velocity components are normalized such that initial amplitude satisfies $|V_x|^2+|V_y|^2+|V_z|^2=1$ in each propagation direction. In the velocity and spectrum plots, the short-dashed, long-dashed, and solid lines correspond to propagation at distances $X=0$, $X=1$, and $X=2$, respectively. The harmonic propagation curves plot the spectral amplitudes $|V_1|$ (solid), $|V_2|$ (long-dashed), $|V_3|$, (short-dashed), $|V_4|$ (dotted), and $|V_5|$ (dot-dashed) as a function of distance.

Finally, this is a pure mode direction, and it may be amenable to measurement.

$\theta=3.2°$: Here $\hat{S}_{11}$ is positive, $\hat{S}_{12}\simeq -4\times10^{-6}$ is close to zero, and $\hat{S}_{13}$ is negative. In addition $\hat{S}_{12}$ is much smaller than $\hat{S}_{11}$ in magnitude ($|\hat{S}_{12}|/|\hat{S}_{11}|\simeq1.5\times10^{-3}$). The matrix element $\hat{S}_{12}$ indicates the coupling strength between the fundamental and second harmonic associated with generation of the third harmonic. The result of the small value of $\hat{S}_{12}$ is highly efficient energy transfer from the fundamental to the second harmonic (because the transfer from the second to the third harmonic is impeded), which in turn causes rapidly depleting energy from the fundamental (see the Appendix of Ref. 1 for additional discussion). The inefficient transfer of energy out of the lowest harmonics leads to other unusual phenomena, including the amplitude of the third harmonic (short-dashed) exceeding the fundamental past $X=5$, and the suppression of fourth harmonic (dotted) around the same location. The complicated interaction of the lowest harmonics is also reflected in the spectra, which exhibit many maxima and minima and also show that relatively little energy is transferred to the higher spectral components. The waveforms do not exhibit shock formation but do show some higher frequency oscillations due to the atypical energy transfer. Additional calculations show that at distances $X>2$ the waveform does not form a shock, and the higher frequency oscillations grow in extent and magnitude. In summary, the simulations identify the $\theta=3.2°$ direction as another direction of shock suppression, although with a still different character than both of those described for Si or for the $\theta=0°$ case in KCl.

$\theta=10°$: Here $\hat{S}_{11}$, $\hat{S}_{12}$, and $\hat{S}_{13}$ are negative but, unlike for $\theta=0°$ and $\theta=35°$ in Si, here the magnitude $|\hat{S}_{11}|$ is less than neighboring elements (e.g., $|\hat{S}_{11}|/|\hat{S}_{12}|\simeq0.84$ and $|\hat{S}_{11}|/|\hat{S}_{12}|\simeq0.68$). This inversion in the magnitudes of the matrix elements causes energy to be transferred to the higher harmonics more efficiently. In turn, this increased rate of energy transfer results in significantly sharper cusping in the waveforms. The harmonic propagation curves also show a steeper decline in the amplitude of the fundamental and a steeper increase in the other harmonics. All directions $10°<\theta<45°$ show this same type of distortion.

Before concluding this section, comments are in order regarding the dependence of the aforementioned results on the choice of third-order elastic constant data. To evaluate the effects of using the same second-order elastic constants but different third-order elastic constants, the nonlinearity matrix elements $\hat{S}_{11}$, $\hat{S}_{12}$, and $\hat{S}_{13}$ corresponding to the data of Drabble and Strathen[32] (used in the KCl simulations above) are plotted together with those of Chang[37] in Fig. 8. Both sets show the same general trend, but the locations of the zero crossings occur for slightly smaller values of θ in the Chang data. Because Hamilton *et al.*[1] used the Chang data to perform their simulations for KCl, their paper shows the kind of waveform distortion seen for $\theta=3.2°$ in this article at $\theta=0°$. An examination of Chang's paper shows that only three of the six TOE constants were determined experimentally (d_{144}, d_{155}, d_{456}) while the other elastic constants

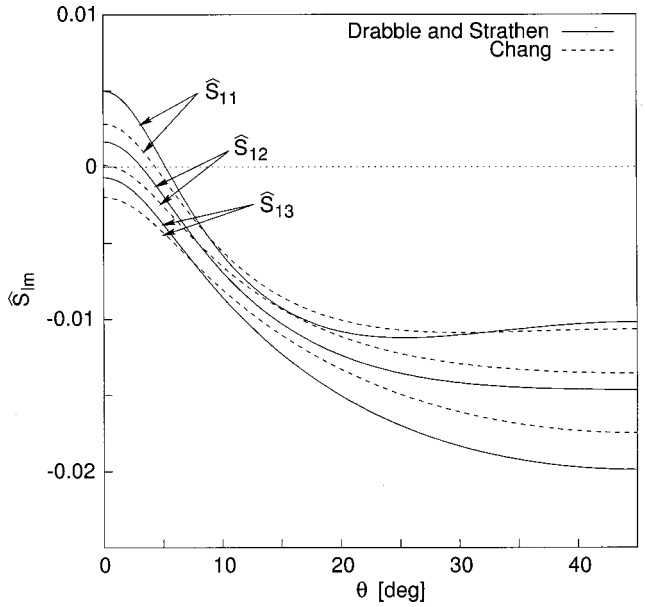

FIG. 8. Comparison of selected nonlinearity matrix elements calculated from third-order elastic constant data of Drabble and Strathen (Ref. 32) and Chang (Ref. 37) for propagation in the (001) plane of KCl. Second-order elastic constant data are taken from Hearmon (Ref. 30) in both cases.

(d_{111}, d_{122}, d_{123}) were computed by assuming the Cauchy relations $d_{123}=d_{456}=d_{144}$ and $d_{112}=d_{166}$. In contrast, Drabble and Strathen measured all six constants and showed that not all the Cauchy relations hold (see Table I). (Although not shown here, a similar comparison[2] was performed for the Si case described in Sec. III B 2. The general trends remain the same although the exact amplitude and zero crossings change by a small amount.) The lesson here is that the nonlinearity matrix elements, and therefore the waveform distortion, can be rather sensitive to changes in the third-order elastic constants. Therefore care should be exercised in making detailed predictions at specific directions without accurate third-order elastic constants.

IV. SUMMARY

This article has investigated the properties of nonlinear SAWs in the (001) plane of selected crystals. Si and KCl were chosen for detailed study. It is found that the nature of the nonlinearity is often very sensitive to changes in direction, and the relative variations can be larger than those occurring in the linear wave speed. For most cases, plotting the first few nonlinearity matrix elements as a function of direction can provide a guide to the nature of the nonlinear effects. While particular directions of high symmetry exhibit harmonic generation and waveform distortion similar to Rayleigh waves, several other effects have been identified. These include the existence of regions of positive and negative nonlinearity within the same cut, several varieties of shock suppression where the generation of particular harmonics is suppressed and shock formation does not occur, and directions in which harmonic generation is increased and energy is more efficiently transferred from the fundamental to higher harmonics. As a result of the last two effects, the simple estimate of the shock formation given by Eq. (14) may not be valid or accurate in some regions. The choice of different

experimental third-order elastic constants as input to the simulations is shown to affect the detailed predictions of the nonlinearity matrix elements in any given direction, but not the general trends over the whole angular range.

ACKNOWLEDGMENTS

This work was supported by the Office of Naval Research. Discussions with Yu. A. Ilinskii and E. A. Zabolotskaya are also gratefully acknowledged.

[1] M. F. Hamilton, Yu. A. Il'inskii, and E. A. Zabolotskaya, "Nonlinear surface acoustic waves in crystals," J. Acoust. Soc. Am. **105**, 639–651 (1999).
[2] R. E. Kumon, "Nonlinear surface acoustic waves in cubic crystals," Ph.D. dissertation, The University of Texas at Austin, 1999.
[3] R. E. Kumon, M. F. Hamilton, P. Hess, A. Lomonosov, and V. G. Mikhalevich, "Dependence of surface acoustic wave nonlinearity on propagation direction in crystalline silicon," in *Nonlinear Acoustics at the Turn of the Millennium*: *Proceedings of the 15th International Symposium on Nonlinear Acoustics*, Vol. 524 of AIP Conference Proceedings, edited by W. Lauterborn and T. Kurz (American Institute of Physics, Melville, NY, 2000), pp. 265–268.
[4] D. F. Parker, "Nonlinear surface acoustic waves and waves on stratified media," in *Nonlinear Waves in Solids*, No. 341 in *International Centre for Mechanical Sciences Courses and Lectures*, edited by A. Jeffrey and J. Engelbrecht (Springer-Verlag, New York, 1994), pp. 289–347.
[5] A. P. Mayer, "Surface acoustic waves in nonlinear elastic media," Phys. Rep. **256**, 237–366 (1995).
[6] M. Planat, "Multiple scale analysis of the nonlinear surface acoustic wave propagation in anisotropic crystals," J. Appl. Phys. **57**, 4911–4915 (1985).
[7] R. W. Lardner, "Nonlinear surface acoustic waves on an elastic solid of general anisotropy," J. Elast. **16**, 63–73 (1986).
[8] R. W. Lardner and G. E. Tupholme, "Nonlinear surface waves on cubic materials," J. Elast. **16**, 251–265 (1986).
[9] D. F. Parker, "Waveform evolution for nonlinear surface acoustic waves," Int. J. Eng. Sci. **26**, 59–75 (1988).
[10] D. F. Parker and E. A. David, "Nonlinear piezoelectric surface waves," Int. J. Eng. Sci. **27**, 565–581 (1989).
[11] M. F. Hamilton, Yu. A. Il'inskii, and E. A. Zabolotskaya, "Nonlinear surface wave propagation in crystals," in *Nonlinear Acoustics in Perspective: Proceedings of the 14th International Symposium on Nonlinear Acoustics*, edited by R. J. Wei (Nanjing U.P., Nanjing, China, 1996), pp. 64–69.
[12] E. A. Zabolotskaya, "Nonlinear propagation of plane and circular Rayleigh waves," J. Acoust. Soc. Am. **91**, 2569–2575 (1992).
[13] E. Yu. Knight, M. F. Hamilton, Yu. A. Il'inskii, and E. A. Zabolotskaya, "General theory for the spectral evolution of nonlinear Rayleigh waves," J. Acoust. Soc. Am. **102**, 1402–1417 (1997).
[14] M. F. Hamilton, Yu. A. Il'inskii, and E. A. Zabolotskaya, "Nonlinear surface acoustic waves," in *Nonlinear Acoustics at the Turn of the Millennium*: *Proceedings of the 15th International Symposium on Nonlinear Acoustics*, Vol. 524 of AIP Conference Proceedings, edited by W. Lauterborn and T. Kurz (American Institute of Physics, Melville, NY, 2000), pp. 55–64.
[15] V. E. Gusev, W. Lauriks, and J. Thoen, "New evolution equations for the nonlinear surface acoustic waves on an elastic solid of general anisotropy," J. Acoust. Soc. Am. **103**, 3203–3215 (1998).
[16] G. D. Meegan, M. F. Hamilton, Yu. A. Il'inskii, and E. A. Zabolotskaya, "Nonlinear Stoneley and Scholte waves," J. Acoust. Soc. Am. **106**, 1712–1723 (1999).
[17] A. Lomonosov and P. Hess, "Laser excitation and propagation of nonlinear surface acoustic wave pulses," in *Nonlinear Acoustics in Perspective: Proceedings of the 14th International Symposium on Nonlinear Acoustics*, edited by R. J. Wei (Nanjing U.P., Nanjing, China, 1996), pp. 106–111.
[18] Al. A. Kolomenskii, A. M. Lomonosov, R. Kuschnereit, P. Hess, and V. E. Gusev, "Laser generation and detection of strongly nonlinear elastic surface pulses," Phys. Rev. Lett. **79**, 1325–1328 (1997).
[19] A. A. Kolomenskii and H. A. Schuessler, "Characterization of isotropic solids with nonlinear surface acoustic wave pulses," Phys. Rev. B **63**, 085413 (2001).
[20] A. A. Kolomenskii and H. A. Schuessler, "Nonlinear compression of giant surface acoustic wave pulses," Phys. Lett. A **280**, 157–161 (2001).
[21] A. Lomonosov and P. Hess, "Effects of nonlinear elastic surface pulses in anisotropic silicon crystals," Phys. Rev. Lett. **83**, 3876–3879 (1999).
[22] A. Lomonosov, V. G. Mikhalevich, P. Hess, E. Yu. Knight, M. F. Hamilton, and E. A. Zabolotskaya, "Laser-generated nonlinear Rayleigh waves with shocks," J. Acoust. Soc. Am. **105**, 2093–2096 (1999).
[23] R. E. Kumon, M. F. Hamilton, Yu. A. Il'inskii, E. A. Zabolotskaya, P. Hess, A. Lomonosov, and V. G. Mikhalevich, "Pulsed nonlinear surface acoustic waves in crystals," in *Proceedings of the 16th International Congress on Acoustics and 135th Meeting of the Acoustical Society of America*, edited by P. K. Kuhl and L. A. Crum (Acoustical Society of America, Woodbury, NY, 1998), Vol. 3, pp. 1557–1558.
[24] G. W. Farnell, "Properties of elastic surface waves," in *Physical Acoustics*, edited by W. P. Mason and R. N. Thurston (Academic, New York, 1970), Vol. 6, pp. 109–166.
[25] M. F. Hamilton and D. T. Blackstock, eds., *Nonlinear Acoustics* (Academic, New York, 1998).
[26] E. Yu. Knight, M. F. Hamilton, Yu. A. Il'inskii, and E. A. Zabolotskaya, "On Rayleigh wave nonlinearity, and analytical approximation of the shock formation distance," J. Acoust. Soc. Am. **102**, 2529–2535 (1997).
[27] M. F. Hamilton, Yu. A. Il'inskii, and E. A. Zabolotskaya, "Local and nonlocal nonlinearity in Rayleigh waves," J. Acoust. Soc. Am. **97**, 882–890 (1995).
[28] W. Pies and A. Weiss, in *Crystal Structure Data of Inorganic Compounds*, *Part a: Key Elements: F, Cl, Br, I*, Vol. III/7a of *Landolt-Börnstein*, New Series, edited by K.-H. Hellwege and A. M. Hellwege (Springer-Verlag, New York, 1973).
[29] P. Eckerlin and H. Kandler, in *Structure Data of Elements and Intermetallic Phases*, Vol. III/6 of *Landolt-Börnstein, New Series*, edited by K.-H. Hellwege and A. M. Hellwege (Springer-Verlag, New York, 1971).
[30] R. F. S. Hearmon, "The elastic constants of crystals and other anisotropic materials," in *Elastic, Piezoelectric, Pyroelectric, Piezooptic, Electroptic Constants, and Nonlinear Dielectric Susceptibilities of Crystals*, Vol. III/11 of *Landolt-Börnstein, New Series*, edited by K.-H. Hellwege and A. M. Hellwege (Springer-Verlag, New York, 1979), pp. 1–244.
[31] D. J. Shull, M. F. Hamilton, Yu. A. Il'insky, and E. A. Zabolotskaya, "Harmonic generation in plane and cylindrical nonlinear Rayleigh waves," J. Acoust. Soc. Am. **94**, 418–427 (1993).
[32] J. R. Drabble and R. E. B. Strathen, "The third-order elastic constants of potassium chloride, sodium chloride and lithium fluoride," Proc. Phys. Soc. London **92**, 1090–1095 (1967).
[33] S. Alterovitz and D. Gerlich, "Third-order elastic moduli of strontium fluoride," Phys. Rev. B **1**, 2718–2723 (1970).
[34] D. Gerlich, "Third-order elastic moduli of barium fluoride," Phys. Rev. **168**, 947–952 (1968).
[35] H. J. McSkimin and P. Andreatch, Jr., "Measurement of third-order moduli of silicon and germanium," J. Appl. Phys. **35**, 3312–3319 (1964).
[36] K. Salama and G. A. Alers, "The composition dependence of the third-order elastic constants of the Cu-Ni system," Phys. Status Solidi A **41**, 241–247 (1977).
[37] Z.-P. Chang, "Third-order elastic constants of NaCl and KCl crystals," Phys. Rev. **140**, 1788–1799 (1965).